




# A synthetic flavonoid derivate in the plasma membrane transforms the voltage-clamp fluorometry signal of CiHv1

Zoltán Pethő<sup>1,2</sup> , Dávid Pajtás<sup>1</sup>, Martina Piga<sup>3</sup> , Zsuzsanna Magyar<sup>4</sup>, Florina Zakany<sup>1</sup>, Tamas Kovacs<sup>1</sup>, Nace Zidar<sup>3</sup>, Gyorgy Panyi<sup>1</sup>, Zoltan Varga<sup>1</sup> and Ferenc Papp<sup>1</sup> 

1 Department of Biophysics and Cell Biology, Faculty of Medicine, University of Debrecen, Hungary

2 Institut für Physiologie II, University of Münster, Germany

3 Department of Pharmaceutical Chemistry, Faculty of Pharmacy, University of Ljubljana, Slovenia

4 Department of Physiology, Faculty of Medicine, University of Debrecen, Hungary

## Keywords

CiHv1; flavonoid derivate; fluorescence-quenching; membrane fluidity; voltage-clamp fluorometry

## Correspondence

F. Papp, Department of Biophysics and Cell Biology, Faculty of Medicine, University of Debrecen, Egyetem ter 1, Debrecen H-4032, Hungary  
 Tel: +3652258603  
 E-mail: [papp.ferenc@med.unideb.hu](mailto:papp.ferenc@med.unideb.hu)

(Received 26 August 2023, revised 28 December 2023, accepted 19 February 2024)

doi:10.1111/febs.17105

Voltage-clamp fluorometry (VCF) enables the study of voltage-sensitive proteins through fluorescent labeling accompanied by ionic current measurements for voltage-gated ion channels. The heterogeneity of the fluorescent signal represents a significant challenge in VCF. The VCF signal depends on where the cysteine mutation is incorporated, making it difficult to compare data among different mutations and different studies and standardize their interpretation. We have recently shown that the VCF signal originates from quenching amino acids in the vicinity of the attached fluorophores, together with the effect of the lipid microenvironment. Based on these, we performed experiments to test the hypothesis that the VCF signal could be altered by amphiphilic quenching molecules in the cell membrane. Here we show that a phenylalanine-conjugated flavonoid (4-oxo-2-phenyl-4H-chromene-7-yl)-phenylalanine, (later Oxophench) has potent effects on the VCF signals of the *Ciona intestinalis* Hv1 (CiHv1) proton channel. Using spectrofluorimetry, we showed that Oxophench quenches TAMRA (5(6)-carboxytetramethylrhodamine-(methane thiosulfonate)) fluorescence. Moreover, Oxophench reduces the baseline fluorescence in oocytes and incorporates into the cell membrane while reducing the membrane fluidity of HEK293 cells. Our model calculations confirmed that Oxophench, a potent membrane-bound quencher, modifies the VCF signal during conformational changes. These results support our previously published model of VCF signal generation and point out that a change in the VCF signal may not necessarily indicate an altered conformational transition of the investigated protein.

## Introduction

Voltage-clamp fluorometry (VCF) is a highly sensitive method for studying the structure–function relationship of voltage-sensitive proteins, including that of voltage-gated ion channels [1,2]. The power of this

technique lies in the fact that it allows the parallel, simultaneous measurement of the ionic current flowing through the ion channel and the change in fluorescence, which indicates a conformational change taking

## Abbreviations

(4-oxo-2-phenyl-4H-chromene-7-yl)-phenylalanine, Oxophench; CiHv1, *Ciona intestinalis* Hv1; G–V, conductance–voltage; HEK293, human embryonic kidney 293 cells; Hv1, voltage-gated proton 1 channel; Kv1.3, voltage-gated potassium 1.3 channel; RCF, remaining current fraction; TAMRA-MTS, 5(6)-carboxytetramethylrhodamine-(methane thiosulfonate); TMA-DPH, trimethylammonium-(1,6-diphenylhexatriene); VCF, voltage-clamp fluorometry.

place in the protein. VCF measurements require an amino acid residue on the extracellular part of the protein to be replaced by a cysteine using site-directed mutagenesis. This cysteine is then labeled with a fluorophore (e.g., TAMRA-MTS) that is sensitive to the local physical–chemical environment. Until recently, fluorescence-quenching amino acids neighboring the fluorophore have been accounted for generating the VCF signal as the major mechanism [3–5]. Introducing a dominant quencher (e.g., a tryptophan) near the fluorophore alters the VCF signal drastically [3,6]. Changes in the membrane potential during VCF measurements result in conformational changes in the voltage-sensitive protein, thereby changing the relative position of the quenching amino acids with respect to the attached fluorophore. Other mechanisms have also been hypothesized to explain the formation of the VCF signal, such as movement of the fluorophore between less polar and aqueous environments [1,2,7], or the electrochromic effect [8–10]. Using the H<sub>v</sub>1 proton channel as a tool, we recently provided evidence that the translocation of the fluorophore from the lipid membrane bilayer toward the aqueous phase extracellular solution during a conformational change is at least as necessary in VCF signal generation as the presence of neighboring quenching residues [6]. The VCF signal generated by quenching amino acids and the lipid environment can be described using a minimal 3-state model [6].

Flavonoids are polyphenolic compounds naturally occurring in plants having a broad spectrum of biological applications. The pharmacological actions of natural flavonoids include antioxidant, antimicrobial, anti-inflammatory, and anti-tumor effects [11]. Based on these effects, some flavonoids are used clinically in various cardiovascular and liver diseases. We tested the biological activity of synthetic flavonoids on multiple cancer cell lines and found that flavone-amino acid hybrids exhibit a marked cytotoxic activity [12]. Due to their usual amphiphilic nature, flavonoids interact with cell membranes both in their hydrophilic and hydrophobic regions [13]. More specifically, they can increase the packing order of lipid heads and decrease membrane fluidity depending on their exact structure and functional groups [14]. This altered fluidity may have a pronounced effect on the activity of transmembrane proteins, e.g., ion channels [15] as demonstrated for the H<sub>v</sub>1 ion channel [16]. Moreover, flavonoids can have a direct impact on ion channels. Various flavonoids act on potassium channels [17], and quercetin, a natural flavonoid, can activate the voltage-gated proton channel H<sub>v</sub>1 [18].

Further biophysical studies of flavonoids show that they can quench the fluorescence of molecules such as diphenyl-1,3,5-hexatriene (DPH), doxorubicin, or tryptophan [19–21]. Prominently, the most potent fluorescence quenchers are planar structures arising from conjugated double bonds and oxo groups. Time-resolved fluorescence decay experiments show that quercetin quenches the amino acid fluorescence of hemoglobin by static quenching, meaning that the compound continuously interacts with the protein [22].

These results led us to investigate the effects of flavonoid molecules on our target ion channel, H<sub>v</sub>1. We hypothesized that amphiphilic flavonoids could affect the H<sub>v</sub>1 proton channel and the VCF signal by binding directly to the ion channel or by incorporating into the cell membrane. To this end, we screened eight compounds for their effect on the *Ciona intestinalis* H<sub>v</sub>1 (CiHv1) channel. We chose H<sub>v</sub>1 as a model ion channel because (a) its transmembrane structure is relatively simple compared to the other larger ion channels [23,24] and (b) the process of VCF signal formation is known in detail [6,25].

## Results

### Effects of flavonoid derivatives on the VCF signal

Figure 1A shows the VCF signal of CiHv1, containing the cysteine mutation E241C and labeled with a thiol-reactive fluorescent compound TAMRA-MTS upon depolarization. The VCF signal is negative and displays a complex temporal progression: a fast quenching component followed by slower dequenching during depolarization, reaching a steady state, then quenching again with greater amplitude resembling a “hook” upon repolarization followed by decay to the fluorescence intensity recorded prior to the voltage step. First, we tested a small compound library of synthetic flavonoid derivatives [12] in a mixture with each component added at 10 μM concentration (Summarized in Fig. 2). Briefly, Mix A consisted of modified flavonoids, where a butylamino (BuNH<sub>2</sub>) group, an anisidine group, or a morpholine group were introduced on C-6 or C-7. Our results indicate that Mix A has a pronounced effect on critical features of the VCF signal (Fig. 1A,C,D, steady state:  $\Delta F_{ss}/F_{h \text{ Ctrl}} = -0.003 \pm 0.001$  a.u.,  $\Delta F_{ss}/F_{h \text{ Mix A}} = 0.009 \pm 0.002$  a.u.,  $P = 0.007$ ; hook:  $\Delta F_{\text{hook}}/F_{h \text{ Ctrl}} = -0.019 \pm 0.006$  a.u.,  $\Delta F_{\text{hook}}/F_{h \text{ Mix A}} = 0.003 \pm 0.002$  a.u.,  $P = 0.028$ ,  $n_{\text{Ctrl}} = 8$ ,  $n_{\text{Mix A}} = 3$  oocytes from  $N \geq 3$  different batches). Since the VCF signal is complex, certain characteristics can be quantified in different ways:  $F_h$  is the fluorescence

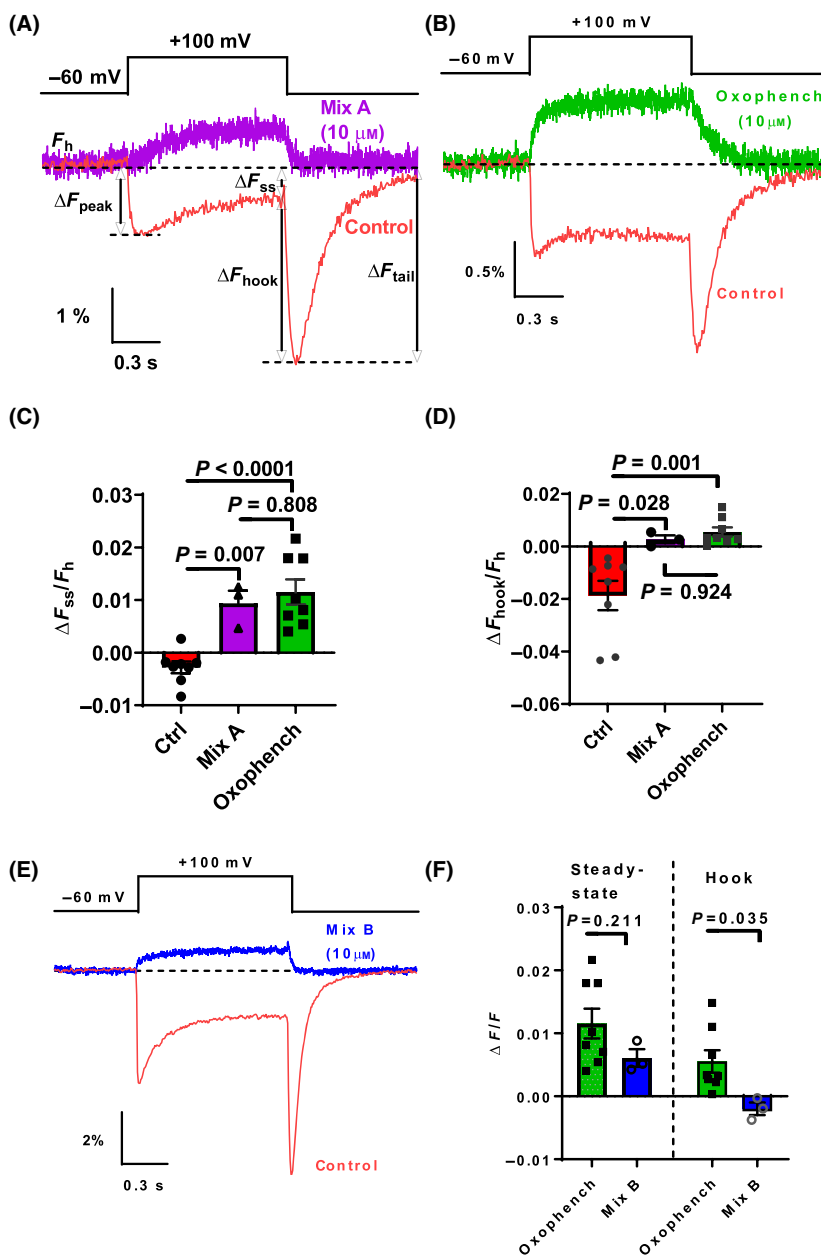


**Fig. 1.** Effect of flavonoid compounds on the fluorescence signal of CiHv1-E241C. Representative fluorescence responses to a depolarization from  $-60$  to  $+100\text{ mV}$ , recorded from *Xenopus* oocytes expressing CiHv1 channels labeled with TAMRA-MTS at the E241C position (red), and exposed to different treatments: Mix A (A), Oxophench (B) and Mix B (E).  $F_h$  is the baseline fluorescence at the holding potential,  $\Delta F_{\text{peak}}$  is negative peak fluorescence change during the voltage step,  $\Delta F_{\text{ss}}$  (steady state) is the change in fluorescence at the end of the voltage step,  $\Delta F_{\text{tail}}$  is the maximum change in fluorescence during repolarization after the voltage step and  $\Delta F_{\text{hook}} = \Delta F_{\text{tail}} - \Delta F_{\text{ss}}$ ; the relative fluorescence change:  $\Delta F/F_h$ , simplified to  $\Delta F/F$ .  $\Delta F_{\text{ss}}/F_h$  and  $\Delta F_{\text{hook}}/F_h$  are quantified in (C) and (D), respectively, and in (F). Representative fluorescence traces were selected from  $n$  oocytes,  $N$  different batches:  $n/N$  control = 8/3,  $n/N$  Mix A = 3/3,  $n/N$  Oxophench = 8/3, (D)  $n/N$  Mix B = 3/3. Data in (C), (D), and (F) represent mean  $\pm$  SEM. Statistical comparison was performed using one-way ANOVA in (C), (D), and with Student's  $t$ -test in (F).

at the holding voltage of  $-60\text{ mV}$ ,  $\Delta F_{\text{peak}}$  is negative peak fluorescence change during the voltage step,  $\Delta F_{\text{ss}}$  (steady state) is the change in fluorescence at the end of the voltage step,  $\Delta F_{\text{tail}}$  is the maximum change in fluorescence during repolarization after the voltage step and  $\Delta F_{\text{hook}} = \Delta F_{\text{tail}} - \Delta F_{\text{ss}}$ ; the relative fluorescence change for any component is defined as:  $\Delta F/F_h$ , later called  $\Delta F/F$ .

The screening was continued by testing the components of the mixture individually. We found that  $10\text{ }\mu\text{M}$  of the phenylalanine-conjugated flavonoid

(4-oxo-2-phenyl-4H-chromene-7-yl)-phenylalanine, termed Oxophench, itself changes the VCF signal to a robust monophasic and positive signal (Fig. 1B–D) (steady state:  $\Delta F_{\text{ss}}/F_h$  Oxophench =  $0.011 \pm 0.002\text{ a.u.}$ ,  $P < 0.0001$ ; hook:  $\Delta F_{\text{hook}}/F_h$  Oxophench =  $0.005 \pm 0.002\text{ a.u.}$ ,  $P = 0.001$ ,  $n = 8$  oocytes from  $N = 4$  different batches). Indeed, the changes in the VCF signal by Mix A are likely to be caused mainly by Oxophench, as their effects are similar (steady state:  $P = 0.808$ ; hook:  $P = 0.924$ ). The progression of the Oxophench-induced VCF signal is characterized by a dequenching component during

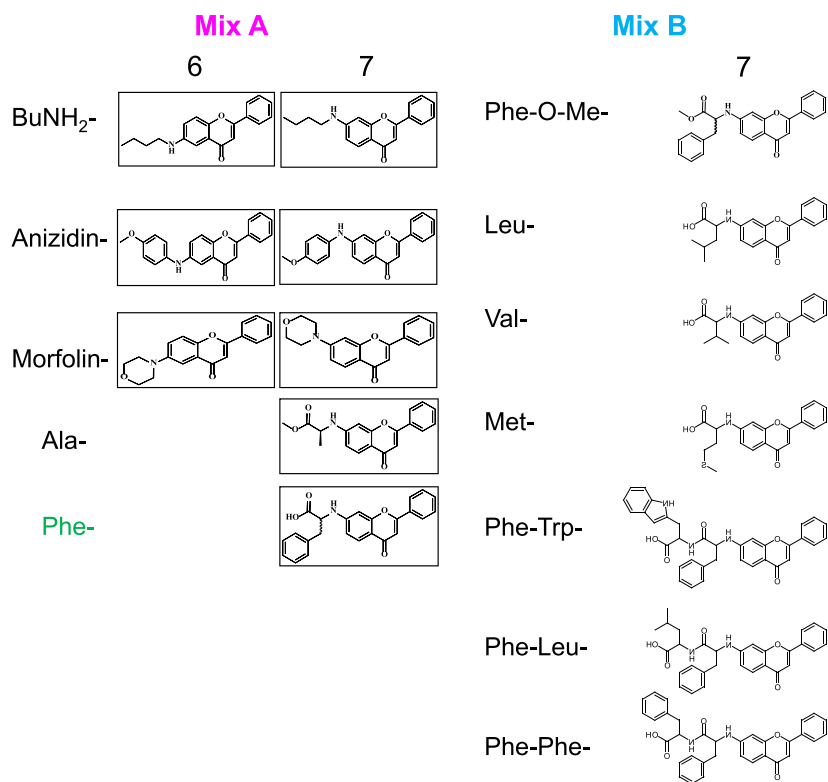


**Fig. 2.** Compound library of synthetic flavonoid derivatives. Mix A on the left side shows the structure of modified flavonoids, where a butylamino (BuNH<sub>2</sub>) group, an anisidine group, or a morpholine group were introduced on C-6 or C-7. Mix B on the right side shows amino acid-conjugated synthetic flavonoid molecules, where C-7 was functionalized with either one amino acid (Leu, Val, Met, Phe-O-Me) or with a phenylalanine-containing dipeptide (Phe-Leu, Phe-Phe, Phe-Trp). The purple, blue, and green colors represent the color coding shown in the other figures, i.e. purple is the color for Mix A, blue for Mix B and green for Oxophench.

depolarization and then quenching upon repolarization that results in a fluorescence decay to the original fluorescence intensity. Despite this drastic change in the fluorescence (becoming a monophasic positive VCF signal from a complex negative signal), the simultaneously measured proton current amplitude at depolarizations to +100 mV remains similar, as shown in Fig. 3D.

Based on the structure of Oxophench, we tested another mixture of related compounds (Mix B), namely amino acid-conjugated synthetic flavonoids from our library (Summarized in Fig. 2) in the same concentration as for Mix A. Mix B contained molecules where C-7 was functionalized with either one amino acid (Leu, Val, Met) or with a phenylalanine-containing dipeptide (Phe-Leu, Phe-Phe, Phe-Trp). The  $\Delta F/F$  values for the steady-state component and the hook for Mix B are shown in Fig. 1E,F, respectively. Since Mix B did not induce more significant changes either in the shape or in the magnitude of the VCF signal of CiHv1 as compared to Oxophench (steady state:  $\Delta F_{ss}/F_h$  Mix B =  $0.006 \pm 0.001$  a.u.,  $P = 0.211$ ; hook:  $\Delta F_{hook}/F_h$  Mix B =  $-0.002 \pm 0.001$  a.u.,  $P = 0.035$ ,  $n = 3$  oocytes from  $N = 3$  different batches), we focused on Oxophench in the rest of the study.

### The phenylalanine-conjugated flavonoid Oxophench modifies the gating of the CiHv1 channel

We next performed an in-depth characterization of the impact of Oxophench on the VCF signal. First, we measured the VCF signals at different Oxophench concentrations (Fig. 3A). At lower concentrations (0.01, 0.1, and 1  $\mu$ M), the complexity and the negative direction of the fluorescence change remained; only the amplitude decreased. At 10  $\mu$ M, the VCF signal became positive and monophasic. Next, we investigated the transformation of the fluorometry signal upon 10  $\mu$ M Oxophench application as a function of time following the application of the compound (Fig. 3B). It is visible that the VCF signal evolves gradually over time, and at 6 min, the signal becomes positive and monophasic (similar to Fig. 1D).

We next performed experiments to assess whether the observed effects on the VCF signal were caused by altered H<sub>v</sub>1 channel gating. When testing the voltage-dependent effects of 10  $\mu$ M Oxophench, we observed a rightward shift in the  $\Delta F_{tail}/F_h$  – voltage ( $F$ – $V$ ) relationship (Fig. 3C;  $V_{1/2} = 46.2$  mV, control;  $V_{1/2} = 50.6$  mV, Oxophench;  $n = 4$  oocytes from  $N = 3$  different batches). This slight shift indicates that the

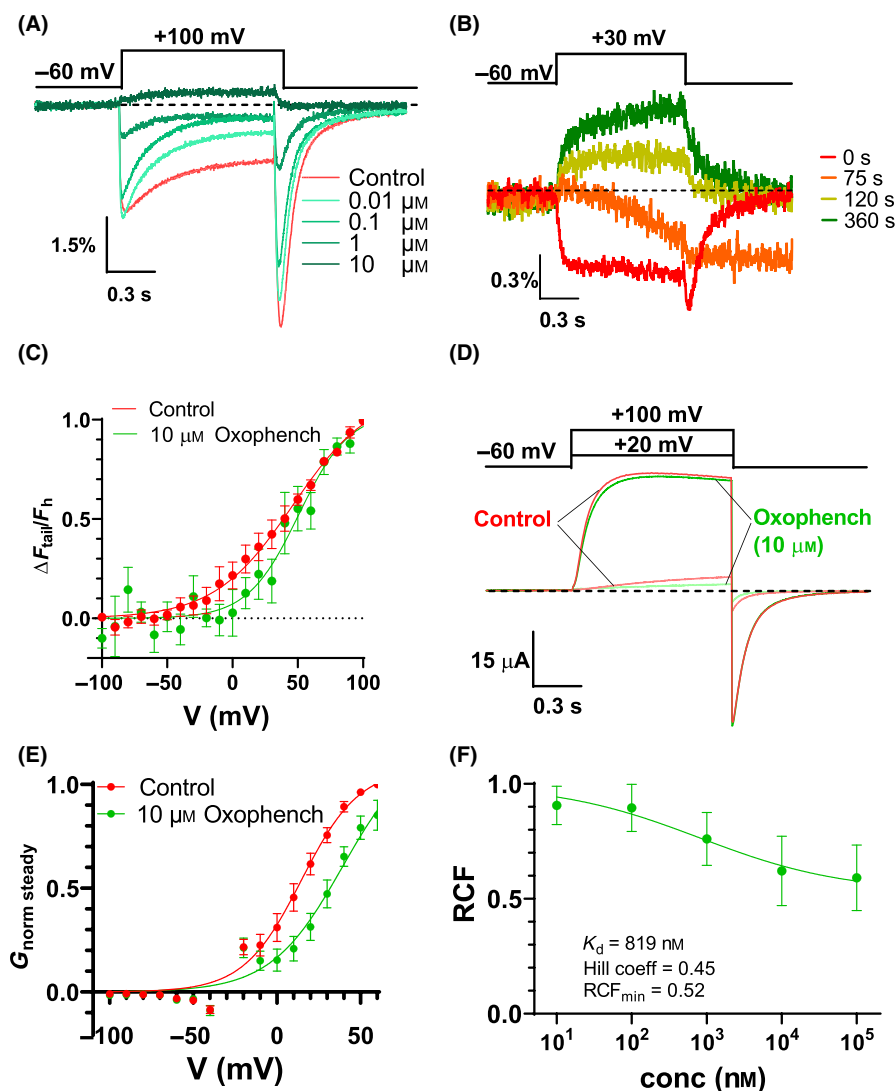


**Fig. 3.** Oxophench acts on the CiHv1 channel in a time-, voltage- and dose-dependent manner. (A) TAMRA-MTS-labeled CiHv1 fluorescence responses to a voltage step from  $-60$  to  $+100$  mV at different concentrations of Oxophench:  $0.01$ ,  $0.1$ ,  $1$ , and  $10$   $\mu\text{M}$ . Darker colors indicate increasing concentrations. The dashed line represents the base line fluorescence value. (B) Representative fluorescence responses upon depolarization from  $-60$  to  $+100$  mV after applying continuous perfusion of  $10$   $\mu\text{M}$  Oxophench. Time points are  $0$  s (red),  $75$  s (orange),  $120$  s (yellow), and  $360$  s (green). The dashed line represents the base line fluorescence value. (C) Voltage-dependence of VCF signal ( $\Delta F_{\text{tail}}/F_h = \Delta F/F_{\text{tail}}$ ) normalized to amplitude measured at  $+100$  mV under control conditions (red) and  $10$   $\mu\text{M}$  Oxophench (green). (D) Proton currents measured at depolarizations to  $+100$  and  $+20$  mV in the absence and presence of  $10$   $\mu\text{M}$  Oxophench (red and green, respectively). The dashed line represents the base line value (proton current is zero). (E) Voltage-dependence of CiHv1 steady-state conductance ( $G$ ) normalized to control conductance value measured  $+60$  mV under control (red) and  $10$   $\mu\text{M}$  Oxophench application (green). (F) Remaining Current Fraction (RCF) was calculated by dividing the peak current at the equilibrium block by the peak current in the absence of Oxophench. The solid line was fitted with a three-parameter inhibitor vs. response equation (see the details in the [Materials and methods](#) section). Representative fluorescence and current traces were selected from  $N=3$  different batches. Lines in (C), (E), and (F) are sigmoidal fits of the indicated data points. Data in (C), (D), and (F) represent mean  $\pm$  SEM.

compound affects the CiHv1 gating, which we followed up by investigating Oxophench effects on the Hv1 currents at different membrane potentials (Fig. 3D). As demonstrated in Fig. 3D, Oxophench effects on the Hv1 current are clearly voltage-dependent, as

Oxophench only elicits an impact at low levels of depolarizations (e.g., to  $+20$  mV) but not when the membrane is fully depolarized (e.g., at  $+100$  mV). The conductance–voltage ( $G$ – $V$ ) relationship (Fig. 3E), derived from the peak current during the depolarization



steps, indicates that Oxophench causes a rightward  $G$ - $V$  shift at  $10\ \mu\text{M}$  concentration ( $V_{1/2\ \text{control}} = 14.6\ \text{mV}$ ,  $V_{1/2\ 10\ \mu\text{M}} = 39.1\ \text{mV}$ ,  $n = 12$  oocytes from  $N = 5$  different batches). There is no data at  $-30\ \text{mV}$  in Fig. 3E since the calculated reversal potential is around this membrane potential. We then tested the concentration-dependence of Oxophench effects on CiHv1 currents between  $0.01$  and  $100\ \mu\text{M}$ . The remaining current fraction (RCF) values were calculated at  $+30\ \text{mV}$  using the current values measured at the end of the depolarization step and plotted as the function of Oxophench concentration (Fig. 3F). The RCF values saturate around  $\text{RCF}_{\text{min}} = 0.52$ , the half-maximal effect is at  $819\ \text{nM}$ , and the Hill coefficient is  $0.45$  ( $n = 6$  oocytes from  $N = 3$  different batches). These results together indicate that Oxophench slightly modifies the gating of H<sub>v</sub>1 in a dose-dependent manner. The rightward shift in the  $G$ - $V$  indicates that Oxophench stabilizes CiHv1 in the closed conformation, i.e., more energy is necessary to open the channel. Consequently, closer to the activation threshold membrane potential, the effect on the proton current is more pronounced. However, this slight, dose-dependent gating modifier effect of Oxophench on the CiHv1 channel is in marked contrast with its pronounced effects on the VCF signal. This becomes evident when depolarizing to  $+100\ \text{mV}$ , where Oxophench does not alter the currents, but the VCF signal becomes monophasic.

### Oxophench incorporates into the cell membrane and quenches TAMRA fluorescence

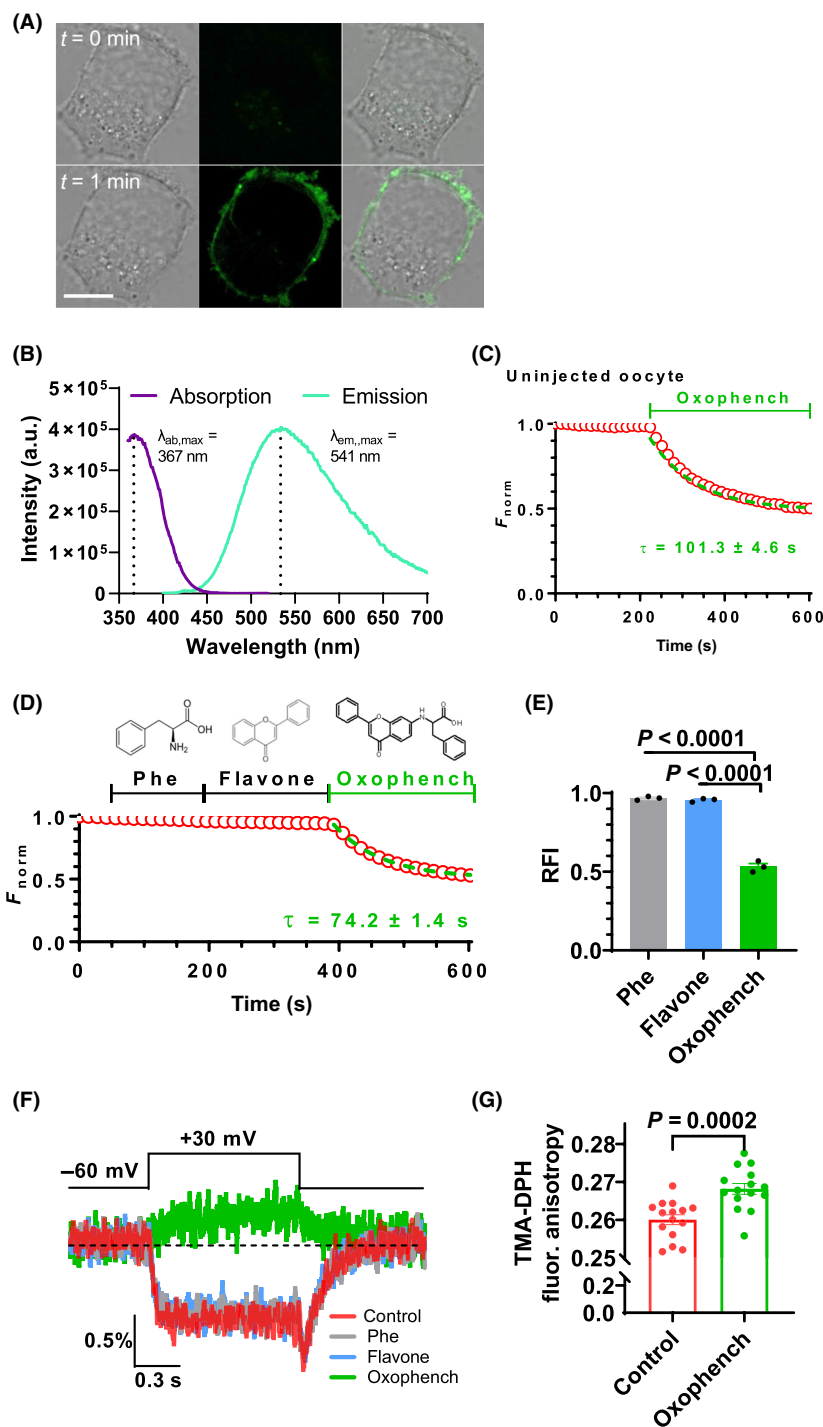
We stated in our recent study that the VCF signal could be altered by quenching amino acids as well as the modified lipid microenvironment near the fluorophore [6]. Structurally, Oxophench is amphiphilic because a hydrophilic backbone of amino acid is attached to a hydrophobic flavonoid backbone. As a quantitative estimate of lipophilicity, we used the

TopP-S tool [26] to predict the  $\text{Log}P$  value of Oxophench, which is  $\text{Log}P = 3.95$ . Due to its amphiphilic nature, we anticipated that Oxophench incorporates into the cell membrane. Testing this hypothesis, first, we exploited that Oxophench itself is fluorescent (Fig. 4B), having an excitation maximum of  $367\ \text{nm}$  and an emission maximum of  $541\ \text{nm}$ . Thus, we visualized HEK293 cells stained with Oxophench (Fig. 4A). Even after just  $1\ \text{min}$ , there is a clear fluorescence signal in the plasma membrane.

Upon measuring the impact of Oxophench on the VCF signal, we observed that Oxophench quenches  $F_h$ , the holding fluorescence measured at  $-60\ \text{mV}$  holding potential (Fig. 4D). We quantified this decrease in fluorescence right after the addition of Oxophench, which can be fitted with a single exponential function with a time constant of  $74.2 \pm 1.4\ \text{s}$  (Fig. 4D). Interestingly, the two constituents of Oxophench, namely phenylalanine and the flavone backbone, do not quench the baseline fluorescence when applied alone, even at  $10$  times higher concentration, at  $100\ \mu\text{M}$  and do not change the magnitude and the shape of the VCF signal (Fig. 4D–F) ( $n = 3$  oocytes from  $N = 3$  different batches,  $F_{\text{Phe}} = 0.97 \pm 0.01\ \text{a.u.}$ ,  $F_{\text{Flavone}} = 0.96 \pm 0.01\ \text{a.u.}$ ,  $F_{\text{Oxophench}} = 0.53 \pm 0.02\ \text{a.u.}$ ,  $P < 0.0001$ ). The Oxophench-induced decay of TAMRA fluorescence is independent of CiHv1, as  $10\ \mu\text{M}$  Oxophench rapidly decreases the fluorescence of TAMRA-labeled, uninjected oocytes (i.e., not injected with RNA, not expressing CiHv1 in the membrane), with a time constant of  $101.3 \pm 4.6\ \text{s}$  (Fig. 4C). This indicates that Oxophench quenches TAMRA fluorophores that attached unspecifically to the oocyte, i.e. to other transmembrane proteins, to the membrane itself, or to the vitelline membrane.

The membrane staining pattern of Oxophench on HEK293 cells and its fluorescence-quenching effects of uninjected frog oocytes point out that the Oxophench incorporates into the cell membrane and thus has a

**Fig. 4.** Oxophench incorporates into the membrane of HEK293 cells and oocytes. (A) Representative confocal microscopy images of HEK293 cells stained with  $10\ \mu\text{M}$  Oxophench for  $1\ \text{min}$  compared to before staining ( $0\ \text{min}$ ). Scale bar =  $10\ \mu\text{m}$ . (B) Excitation (purple) and emission (green) spectra of Oxophench (C) TAMRA holding fluorescence ( $F_h$ ) of stained, uninjected oocytes (not expressing CiHv1) normalized to the fluorescence value measured at the initial time point, before and after  $10\ \mu\text{M}$  Oxophench perfusion. (D) TAMRA holding fluorescence ( $F_h$ ) of stained oocytes expressing CiHv1-E241C normalized to the fluorescence value measured at the initial time point. Substances applied are  $100\ \mu\text{M}$  phenylalanine (Phe),  $100\ \mu\text{M}$  flavone backbone (flavone) and  $10\ \mu\text{M}$  Oxophench. (E, F) Quantification and representative VCF signals of data represented in (C). (F) Effects of  $10\ \mu\text{M}$  Oxophench on TMA-DPH fluorescence anisotropy inversely related to membrane fluidity as determined using spectrofluorimetry. Representative fluorescence data points in (C) and (D) were selected from  $n = 3$  measurements. The green dashed lines in (C) and (D) are exponential fits to the indicated data points. Data in (E) ( $n = 3$ ) represent mean  $\pm$  SEM, with statistical comparison performed using one-way ANOVA. Data in (G) represent mean  $\pm$  SEM of  $n = 15$  biological replicates from three independent experiments, with statistical comparison performed using Student's  $t$ -test.



close proximity to the TAMRA bound specifically or non-specifically to the SH groups of membrane proteins (to CiHv1 or native membrane proteins, respectively). Given that Oxophench belongs to the group of flavonoids that often modify membrane structure [14], to further support its membrane embedding that could

result in modified TAMRA signals, we performed TMA-DPH fluorescence anisotropy measurements to quantify changes induced by this compound in membrane fluidity on HEK293 cells [27,28]. In these experiments, Oxophench significantly increased anisotropy of the environment-sensitive fluorophore when compared

to control samples ( $0.260 \pm 0.0013$  vs.  $0.268 \pm 0.0014$ ,  $n = 15$ ,  $P = 0.0002$ , Fig. 4G) referring to reduced membrane fluidity. These results confirm that Oxophench incorporates into the membrane, presumably in the vicinity of the TAMRA fluorophore thereby altering its fluorescent properties (see also Fig. 5A). Furthermore, embedding of Oxophench into the bilayer and consequent changes in lipid packing can also contribute to the observed slight, dose-dependent modifier

effect of Oxophench on Hv1 gating in oocytes described above (Fig. 3C–F).

### Oxophench modifies the VCF signal during conformational changes by being a strong membrane-bound quencher near TAMRA

Above, we showed that Oxophench changes the VCF signal of CiHv1 (Fig. 1), slightly alters channel gating

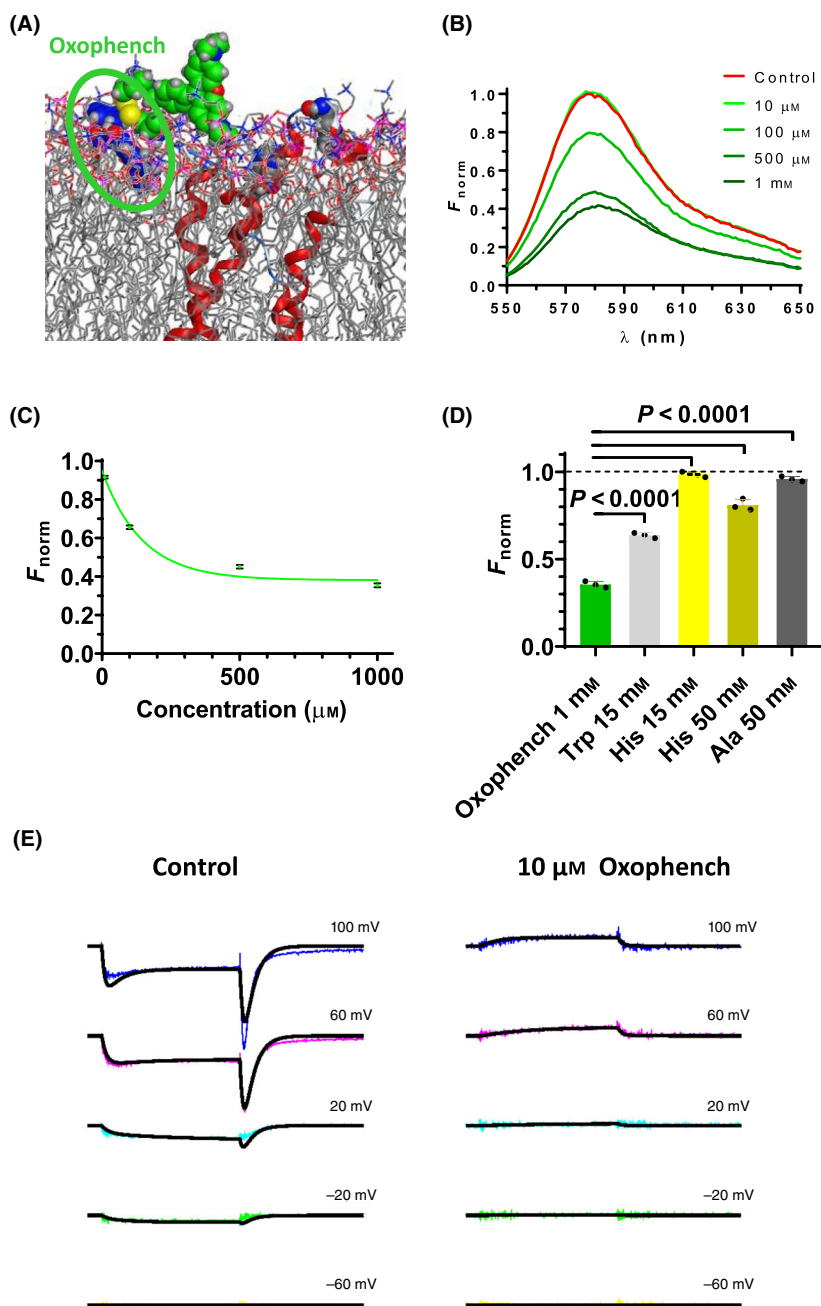




**Fig. 5.** Oxophench quenches TAMRA fluorescence. (A) Representative caption of a molecular docking experiment with Oxophench (blue molecule, highlighted in green ellipse) docked into the extracellular POPC membrane bilayer leaflet (gray) in the vicinity of TAMRA-MTS (green molecule) bound to CiHv1 (red) at position E241C. This figure was generated by using UCSF CHIMERA X and AUTODOCK (details are in the [Materials and methods: Molecular modeling](#)) (B) Representative spectrofluorimetric TAMRA-MTS fluorescence under control (red) or in the presence of Oxophench (green): 10  $\mu\text{M}$ , 100  $\mu\text{M}$ , 500  $\mu\text{M}$ , and 1 mM. Darker colors indicate increasing concentrations. (C) Fluorescence intensity ( $F$ ) relative to control ( $F_0$ ) as a function of wavelength at different Oxophench concentrations ( $F/F_0$  vs  $\lambda$ ) (SEM is indicated by black lines,  $N=3$ ). (D) Fluorescence intensities normalized ( $F_{\text{norm}} = F/F_0$ ) to control (dashed line) in the presence of 1 mM Oxophench (green), 15 mM tryptophan (Trp, gray), 15 and 50 mM histidine (His, yellow and orange), and 50 mM alanine (Ala, black). (E) Solid black lines represent common three-state kinetic model calculation of VCF signal generation under control (left) and 10  $\mu\text{M}$  Oxophench (right) at different membrane potentials (from  $-60\text{ mV}$  up to  $+100\text{ mV}$ ), compared to experimental traces (colored lines). Fluorescence Representative graphics, traces, and models in (A), (B), and (E), respectively, were selected from  $n=3$  measurements. Solid green line in (C) is an exponential fit to the indicated data points. Data in (C) and (D) ( $N=3$ ) represent mean  $\pm$  SEM, with statistical comparison in (D) performed using one-way ANOVA.

(Fig. 3), and that the compound interacts with or inserts into the plasma membrane (Fig. 4). We hypothesized that there is a direct, causative correlation between these effects: Oxophench acts as a membrane-associated quencher which is dominant over the endogenous histidine quenchers in Hv1 (H179 and H188 in the CiHv1) upon conformational changes. That would explain why the biphasic signal is changed to a monophasic one. To test this hypothesis, we first assessed whether molecular proximity is plausible between membrane-localized Oxophench and CiHv1 labeled with TAMRA. We created a homology model of the TAMRA-coupled CiHv1 E241C mutant in a POPC model membrane. Next, we performed a molecular docking experiment with Oxophench as a ligand (Fig. 5A). Indeed, Oxophench acquires a favorable position in the vicinity of TAMRA in the plasma membrane. Thus, it is conceivable that the two molecules get into close proximity during a conformational change.

To investigate whether Oxophench can be a dominant quencher over H179 and H188, we measured how Oxophench quenches TAMRA in a cell-free environment in a spectrofluorimeter cuvette. Here, we found that Oxophench quenches TAMRA fluorescence in a dose-dependent manner (Fig. 5B,C), with its effects saturating at 1 mM with a remaining TAMRA fluorescence of  $34 \pm 1\%$  ( $n=3$ ). Then, we compared Oxophench effects on TAMRA to the strong quencher Trp, the weak quencher His, and the non-quencher Ala (Fig. 5D). Indeed, Oxophench in 1 mM concentration is a stronger quencher than His at 15 or 50 mM, with remaining TAMRA fluorescence values of  $99 \pm 1\%$ ;  $n=3$  and  $81 \pm 2\%$ ;  $n=3$ , respectively. Similarly, Oxophench in 1 mM concentration is a stronger quencher than Trp at 15 mM or Ala in 50 mM concentrations with remaining TAMRA fluorescence values of  $64 \pm 1\%$ ;  $n=3$ , and  $99 \pm 1\%$ ;  $n=3$ , respectively.

According to the same three-state model that we published in our previous article [6], if a prominent quencher such as Oxophench is present, the TAMRA fluorophore is greatly quenched in the vicinity of the quencher. When TAMRA moves away from the quencher during depolarization, the VCF signal becomes monophasic and positive (the fluorescence increasing) (Fig. 5E).

### Mutant CiHv1 constructs recapitulate the mechanism of action of Oxophench

To confirm this model prediction, we tested how CiHv1 mutants, where H179 and H188 are mutated to Trp, alter the VCF signal in the presence of Oxophench (Fig. 6A). Generally, the mutation of two His residues to Trp (H179W/H188W) yields a much greater VCF signal amplitude and therefore a much better signal-to-noise ratio (Fig. 6A) [6]. In addition, the shape of the VCF signal for this mutant CiHv1 construct is also different from wild-type Hv1: upon depolarization, there is a fast quenching component which is followed by a slower and greater quenching (and not dequenching as for the H179/H188 construct in Fig. 1A). Upon repolarization, there is a single dequenching component, and the fluorescence returns to the initial intensity. In the presence of 10  $\mu\text{M}$  Oxophench, the VCF signal amplitude of H179W/H188W becomes a monophasic positive signal ( $\Delta F_{\text{ss}}/F_{\text{h Ctrl}} = -0.096 \pm 0.021$  a.u.,  $\Delta F_{\text{tail}}/F_{\text{h Oxophench}} = 0.008 \pm 0.001$  a.u.,  $P=0.001$ ,  $n=5$  oocytes from  $N=3$  different batches) (Fig. 6E), reminiscent of how Oxophench affects the VCF signal of the H179/H188 construct. This result indicates that the quenching of the fluorophore by Oxophench dominates over the strong Trp quencher during the VCF signal formation. Oxophench had no significant effect on the ionic current, similar to the case of the WT channel (Fig. 6B).

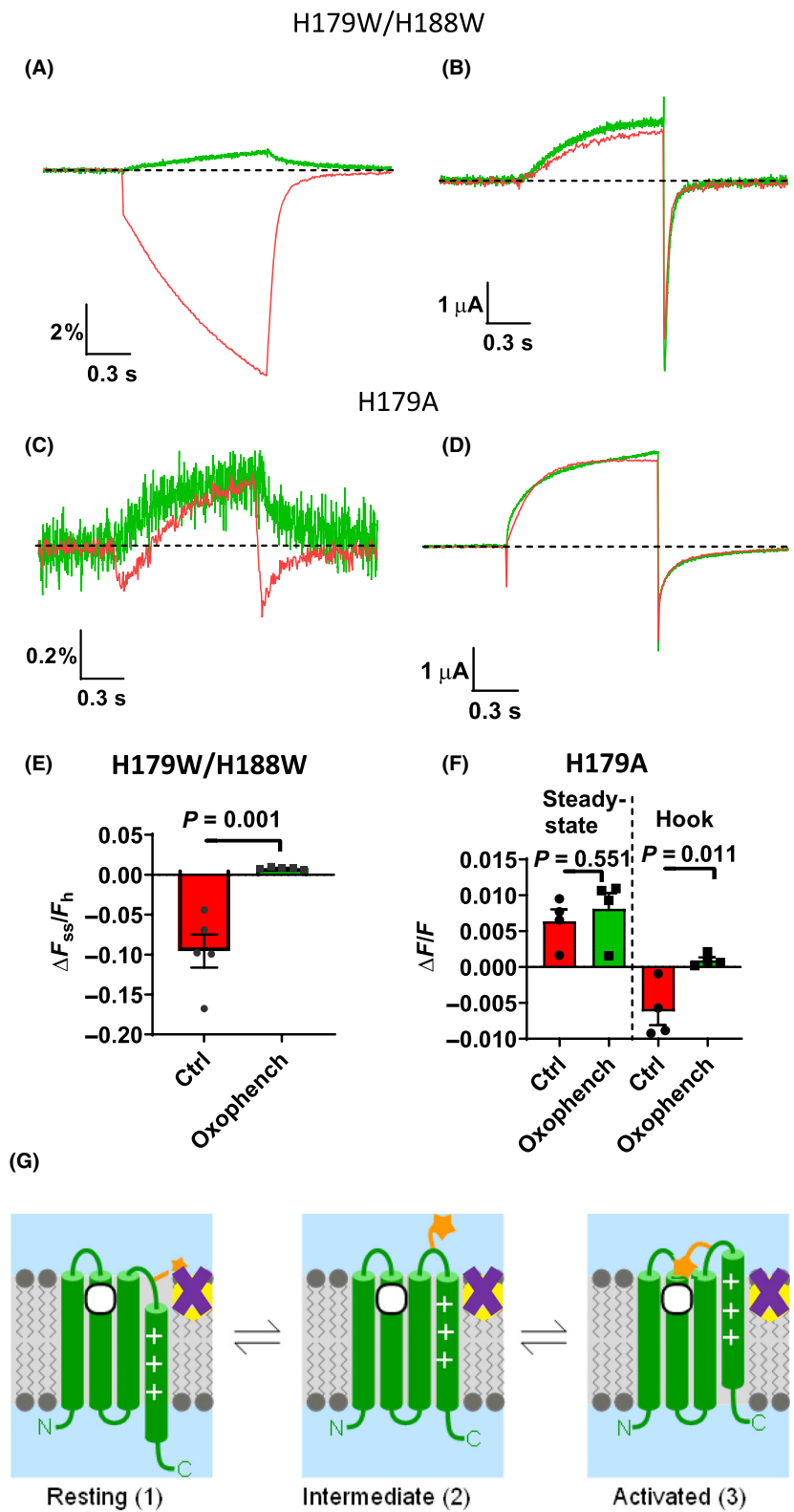


**Fig. 6.** Oxophench affects VCF signal in quencher-mutant CiHv1-E241C constructs. (A–D) Representative fluorescence responses (A, C) and proton currents (B, D) to a voltage step from  $-60$  to  $+100$  mV, under control (red) and  $10\ \mu\text{M}$  Oxophench (green) from oocytes labeled with TAMRA-MTS, expressing Ci-Hv1 E241C containing the following mutations: H179W/H188W (A, B), H179A (C, D). (E, F) Quantification of steady-state and hook  $\Delta F/F$  under control (red) and  $10\ \mu\text{M}$  Oxophench (green). (G) Working model of Oxophench (purple X) on the VCF signal: the model assumes two major VSD (Voltage-Sensitive Domain; green) movements among three states traced by the attached TAMRA (orange star). The resting (1), the intermediate (2) and the activated (3) states are associated with different fluorescence intensities (symbolized by different size of orange star. Smaller size represents less fluorescence). TAMRA is in close proximity to the membrane, and thus Oxophench, in the resting state (1). This leads to TAMRA quenching since Oxophench has strong quenching ability. Upon depolarization, TAMRA first moves away from the lipid bilayer and the quencher Oxophench from state (1) to (2), leading to dequenching. Subsequently, there is a second motion from state 2 to 3, when the dye approaches the lipid bilayer and a quenching His or point-mutated Trp residue (white circle), but at the same time moves further away from Oxophench and thus fluorescence further increases. Representative fluorescence and current traces were selected from  $n$  oocytes/ $N$  different batches: H179W/H188W:  $n/N$  control = 5/3,  $n/N$  Oxophench = 5/3; H179A:  $n/N$  control = 4/3,  $n/N$  Mix A = 4/3. Data bars in (E) and (F) represent mean  $\pm$  SEM, with statistical comparison performed using Student's  $t$ -test.

Based on the results above, we postulated that the fluorescence of TAMRA is primarily affected by Oxophench and not the endogenous quenching amino acids. In that case, the substitution of an endogenous quencher His to a non-quencher amino acid should not affect the VCF signal measured in the presence of Oxophench. Thus, we tested the impact of Oxophench on the H179A mutant (Fig. 6C,D,F). Indeed, we observed a similar positive monophasic signal in the presence of Oxophench as for the wild-type or the Trp substituted constructs ( $\Delta F_{\text{ss}}/F_{\text{h Ctrl}} = 0.006 \pm 0.002$  a.u.,  $\Delta F_{\text{tail}}/F_{\text{h Oxophench}} = 0.008 \pm 0.002$  a.u.,  $P = 0.551$ ;  $\Delta F_{\text{hook}}/F_{\text{h Ctrl}} = -0.006 \pm 0.002$  a.u.,  $\Delta F_{\text{tail}}/F_{\text{h Oxophench}} = 0.001 \pm 0.001$  a.u.,  $P = 0.011$ ,  $n = 4$  oocytes from  $N = 3$  different batches). These results recapitulate the predictions of our model (Fig. 5E), thereby reinforcing that Oxophench inserts into the plasma membrane near Hv1 and modulates the VCF signal by quenching as TAMRA moves relative to Oxophench during the voltage-dependent conformational changes of the Hv1 channel (Fig. 6G).

## Discussion

This study highlights the amphiphilic phenylalanine-coupled flavonoid molecule termed Oxophench. The effects of Oxophench can be summarized in three points: (a) it substantially alters the shape and direction of the VCF signal; (b) it has a strong fluorescence-quenching effect in a cuvette and during VCF measurements; (c) it indirectly modifies the gating of the CiHv1 ion channel by binding to the lipid bilayer of the cell membrane. However, based on these experiments, we cannot exclude the possibility of direct binding to Hv1 either. We could link these phenomena in this study together: by binding to or residing in the plasma membrane (Figs 4 and 5A), Oxophench can

potently quench TAMRA fluorescence when the fluorophore is in close vicinity of Oxophench at negative membrane potentials (Figs 1 and 5E). However, upon depolarization, the fluorophore moves away from Oxophench causing a dequenching. In addition, it can be assumed that the embedding of Oxophench in the membrane alters certain biophysical parameters of the cell membrane and thereby indirectly modifies the gating mechanism of Hv1. Among the biophysical parameters, fluidity was investigated, and it was obtained that the embedding of Oxophench significantly reduces the fluidity of the cell membrane (Fig. 4G). This hypothesis is in accordance with previous studies demonstrating that altered packing in the cell membrane can modulate the gating process of various voltage-gated channels [15]. It was previously reported that increased membrane fluidity increases the proton current through Hv1 measured at a given membrane potential, since the activation of the proton current is accelerated and the  $G$ - $V$  function is shifted to the left indicating that Hv1 opens at a more negative membrane potential [16]. This is in good agreement with our results, since decreased membrane fluidity induced by Oxophench resulted in a slight inhibitory effect on the Hv1 current in a dose-dependent manner at a given membrane potential (Fig. 3C–F).

As we showed in our previous study, the VCF signal is generated by the combined effects of lipids during the movement of the dye relative to the plane of the membrane and by quenching amino acids. Here, we introduce Oxophench as a tool compound to consider when performing VCF measurements. Regardless of the quenching nature of the adjacent amino acids at positions 179 and 188 (Figs 1B–D and 6A–D), the VCF signal becomes a monophasic positive signal. In the H179W/H188W and the H179A mutants, the monotonical increase in fluorescence in the presence of

Oxophench indicates two things: (a) Oxophench has a stronger quenching effect on TAMRA than the Trp or Ala residues (Fig. 5D). (b) The double Trp (H179W/H188W) and the H179A mutant Hv1 channels go through very similar conformational change: the TAMRA dye moves along a very similar path during depolarization as the WT since the VCF signals look very similar in the presence of Oxophench in all these constructs when the TAMRA is attached to the 241C position (Figs 5E and 6A,C,G). Obviously, it also follows that if the dye molecule were bound to cysteine in a different position (e.g. 242C), TAMRA would also move along a different path. Therefore, the VCF signal would have a different shape (see the different VCF signal shapes when cysteine in position 241 or 242 was labeled with fluorescent dye in the Qiu *et al.* article [25]). Thus, we propose the application of Oxophench during VCF measurement of other membrane proteins to become the dominant determinant of the VCF signal. Thereby, Oxophench would inform about the distance of the dye to the plasma membrane and would provide information on an extra dimension facilitating the more precise description of the trajectory of the fluorophores during protein conformational changes.

Oxophench acts as the active substance in our mixture containing eight flavonoid derivatives (Mix A, Fig. 1A–D). The amphiphilic nature of this compound is apparent compared to other substances in the mixture, as Oxophench contains a hydrophobic flavone backbone, with the C7 coupled to a hydrophilic backbone of amino acid. Indeed, we confirmed that Oxophench but not its individual components incorporate into the plasma membrane (Fig. 4). We gained important insights into the mechanism of Oxophench by comparing it with other amphiphilic flavonoids (Mix B, Figs 1E,F and 2). Mix B contains substances with potential structural optimizations by either changing the amino acid coupled to the flavone backbone or by conjugating the backbone with a dipeptide with differential quenching properties: Ala acts as a non-quencher whereas Trp is a strong quencher (Fig. 5D) [6,29]. However, we found that Mix B, where modifications included a Trp side chain, does not enhance effects on the VCF signal compared to Oxophench alone. This implies that the flavone backbone, and not the Phe, quenches the VCF signal. However, the flavone backbone needs to be conjugated in order to affect the VCF signal, as the flavone backbone alone is not sufficient to quench the TAMRA fluorophore in our VCF measurements (Fig. 4D,E). Moreover, the fact that dipeptides in Mix B failed to improve quenching effects may point to a size restraint of the flavonoid quencher.

Our results confirm our model for the generation of the VCF signal and the conformational change of CiHv1 published recently [6], namely that the VCF signal formation is primarily determined by quenching if a dominant quencher is present in the close vicinity of the fluorophore. On the other hand, the double Trp, the H179A mutants and the WT Hv1 go through similar conformational changes despite the large difference in their VCF signals. This is not surprising since it is the same CiHv1 ion channel in all cases; the only difference is that the VCF signal is determined by different factors in the different constructs. Therefore, as a starting point, we took our recently published model [6], from which we constructed the model shown in Fig. 6G. These panels refer to the fluorescence changes in the presence of Oxophench (purple X). The movement of TAMRA is the same here as in our published model [6]. Here, Oxophench is embedded in the lipid bilayer, which primarily determines the fluorescence of the TAMRA dye. During depolarization, TAMRA moves continuously away from the strong quencher Oxophench, and consequently, the fluorescence increases continuously. This is a minimal 3-state model (Resting (1)  $\leftrightarrow$  Intermediate (2)  $\leftrightarrow$  Activated (3)) [6,25], which can describe the conformational changes of Hv1, the pathway of TAMRA, and the generation of the VCF signal. This simple 3-state model fits the VCF signal well in the presence and the absence of Oxophench, as shown in Fig. 5E.

The strong quenching effect of Oxophench on TAMRA fluorescence was proven by spectrofluorimetry in a cuvette (Fig. 5B–D) and on frog oocytes by VCF (Fig. 4C–F). It is also true that no quenching effect was seen in cuvettes at the concentration (10  $\mu\text{M}$ ) at which the VCF technique was detecting a maximum quenching effect. Similar fluorescence quenching could only be measured in cuvettes at 50 times higher concentration (500  $\mu\text{M}$ ). This can be explained by the fact that when measured in cuvettes, both TAMRA and Oxophench were present in a water-soluble form, i.e., they were free to move. In contrast, when measured in oocytes with VCF, both TAMRA and Oxophench were present in bound form. That is, TAMRA was bound to the free SH- group of Cys in CiHv1, whereas Oxophench was embedded in the lipid bilayer. If Oxophench was embedded in the membrane in the vicinity of TAMRA, this could be interpreted as if the local concentration of Oxophench around TAMRA was high. This is also indicated by the fact that the quenching effect required time in the VCF experiments ( $\tau = 74.2$  s, Fig. 4C,D), whereas in the spectrofluorimetric measurement, the effect was instantaneous. That is, time was needed for a sufficient amount of

Oxophench molecules to accumulate in the membrane around TAMRA and to decrease the baseline fluorescence ( $F_h$ ) of the VCF measurement.

The finding that Oxophench quenches the fluorescence of TAMRA-labeled uninjected oocytes by 50% indicates that the Oxophench molecule does not primarily exert its effect by binding directly to H<sub>V</sub>1 (Fig. 4C). Uninjected oocytes can also be stained with TAMRA, since oocytes can express proteins in their membrane that contain extracellularly available cysteine residues. In this case, applying Oxophench in the extracellular solution resulted in a similar decrease in baseline fluorescence in uninjected oocytes as in oocytes expressing CiHv1. But it should also be noted that since the fluorescence reduction is the same for both injected and uninjected oocytes, it follows that Oxophench not only reduces non-specific (background) fluorescence, but also indiscriminately reduces specific fluorescence, i.e. the fluorescence of the TAMRA molecules that are bound to CiHv1 and that provide the VCF signal. This, together with the high  $\text{Log}P$  value and the alteration of membrane fluidity, leads to the conclusion that Oxophench does not directly bind to CiHv1 but rather to the lipids in the *Xenopus* oocyte membranes. Further confirmation of the membrane binding is provided by HEK293 cells stained with Oxophench (Fig. 4A). Incidentally, the membrane-bound Oxophench is close enough to TAMRA attached to CiHv1 to exert its dominant quenching effect. However, the fact that the fluorescence of non-specifically bound TAMRA dyes is also quenched by Oxophench does not influence the shape and size of the voltage-dependent conformational change-generated VCF signal, and thus does not affect our conclusions.

We also observed that in the presence of Oxophench, the proton flux through CiHv1 decreased and a rightward shift was measured in the conductance-voltage relationship ( $G-V$ ) in a concentration-dependent manner (Fig. 3C,D,F). Plotting the RCF as a function of concentration (Fig. 3F) and fitting with the Hill-equation (see [Materials and methods](#)), a Hill coefficient of 0.45 was obtained. This Hill coefficient, together with our results with uninjected oocytes and with HEK293 cells (Fig. 4), indicate that the Oxophench effect on H<sub>V</sub>1 currents is indirect. We postulate that Oxophench binds to the cell membrane and changes the biophysical parameters of the membrane as mirrored by the decreased membrane fluidity (Fig. 4G). This altered membrane fluidity results in an altered function of membrane proteins – and thus of the H<sub>V</sub>1 ion channel [16] as observed in other voltage-gated ion channels [15]. Consistently, it is reasonable

to assume that in this more rigid medium, the conformational change of the H<sub>V</sub>1 ion channel requires more energy as we previously showed in the case of K<sub>V</sub>1.3 [30]. This assumption is also supported by the rightward shift of the  $G-V$  function (Fig. 3E) in the presence of Oxophench. Summarizing all our observations we conclude that the greatly altered VCF signal does not indicate that CiHv1 gating or voltage-sensing ability has changed in the presence of Oxophench. The big change in the VCF signal is due to the fact that Oxophench, a very strong, dominant fluorescence-quenching molecule, was bound near the TAMRA dye and thereby determines and changes the shape of the VCF signal during the conformational change of CiHv1. When Oxophench is not present (control), the shape of the VCF signal is determined by the relative distance between TAMRA and the lipid molecules of the cell membrane, as well as the amino acids (His and/or Trp) capable of quenching the fluorescence. The model for the motion of TAMRA during the conformational change can be seen in Fig. 6G. The decrease in the current flowing through CiHv1 is an indirect effect of Oxophench, as the change in the fluidity of the cell membrane could have caused the decrease in current, not the direct binding of Oxophench to CiHv1.

Our results also draw attention to the fact that when molecules with potential or proven modulatory actions on a specific ion channel (for example, potential ion channel inhibitor small molecules, antagonists, or agonists) are applied extracellularly during VCF measurements then the results obtained in this way must be interpreted with great care because the given molecule may have a direct effect on the fluorophore used for VCF. Thus, the observed change in the VCF signal may not be the result of the conformational change of the ion channel but that of the direct (quenching) effect.

## Materials and methods

### Molecular biology, expression systems

This method has been described in our earlier paper [6]. Briefly: the plasmid encoding the CiHv1 containing the cysteine mutation E241C was generously provided by Peter Larsson (Univ. Miami). The Trp mutations (H179W, H188W) were constructed via site-directed mutagenesis using an overlapping PCR procedure, and the mutations were verified by sequencing. *Xenopus laevis* oocytes were purchased from EcoCyte Bioscience (Dortmund, Germany). Oocytes were injected with 50 nL of RNA and incubated at 18 °C for 2–5 days. Chemicals used for the preparation of



the solutions were purchased from Sigma-Aldrich (St. Louis, MO, USA).

### Synthesis of Oxophench and related compounds

(4-Oxo-2-phenyl-4*H*-chromen-7-yl) phenylalanine (compound termed Oxophench) and flavonoid compounds summarized in Fig. 2 were synthesized as described previously [12]. Briefly, Oxophench synthesis was performed from 3-bromophenol in six reaction steps according to the procedures described in supplementary scheme 1. in Pajtas's article. Reagents and solvents were purchased from Acros Organics (Geel, Belgium), Apollo Scientific (Stockport, UK), Fluorochem (Derbyshire, UK), Sigma-Aldrich, and TCI (Tokyo, Japan), and used without further purification. Analytical TLC was performed on silica gel Merck 60 F<sub>254</sub> plates (0.25 mm), using visualization with UV light and spray reagents. Column chromatography was carried out using Kieselgel 60 as stationary phase, with a granulometry of 0.040–0.063 nm (230–400 mesh ASTM). <sup>1</sup>H and <sup>13</sup>C NMR spectra were recorded at 400 and 100 MHz, respectively, on a Bruker AVANCE III 400 spectrometer (Bruker Corporation, Billerica, MA, USA) in DMSO-*d*<sub>6</sub> or CDCl<sub>3</sub> solutions, with TMS as the internal standard. The purity of the prepared compounds was monitored by liquid chromatography using method A (see supplementary material of Pajtas's article) on a 1260 Infinity II LC system (Agilent Technologies, Santa Clara, CA, USA) equipped with a quaternary pump and a wavelength detector. The system was coupled with mass spectrometry (Expression CMS<sup>L</sup>; Advion Inc, Ithaca, NY, USA). HRMS analysis was performed on a VG Analytical Autospec Q mass spectrometer (Fisons, VG Analytical, Manchester, UK).

### Voltage-clamp fluorometry

This method has been described in our earlier paper [6]. Oocytes were labeled for 20–40 min, at 13 °C with 10 μM of TAMRA-MTS (Toronto Research Chemicals, Toronto, ON, Canada), diluted in ND93 solution. Fifty nanoliter of 1 M HEPES (pH = 7.0) was injected into each oocyte prior to labeling to minimize pH changes due to the proton efflux during recording. The extracellular solution for CiHv1 recordings contained (in mM) 75 NaCl, 2 CaCl<sub>2</sub>, 1 EGTA, and 100 HEPES, pH 7.5, and the intracellular solution contained 3 M KCl. Ionic currents were recorded with an Oocyte Clamp OC-725C amplifier (Warner Instruments, Hamden, CT, USA). VCF signals were acquired through a 40×, 0.8-NA CFI Plan Fluor Nikon fluorescence water-immersion objective on a Nikon Eclipse FNI microscope (Nikon, Tokyo, Japan) and a photodiode (PIN-040A; United Detector Technology, OSI Optoelectronics, Hawthorne, CA, USA). Illumination was provided by a green LED (530 nm), M530L2-C1 from ThorLabs (Newton, NJ,

USA). TAMRA-MTS signals were recorded using a 545/25 excitation filter, a 565LP dichroic mirror and a 605/70 emission filter. The signal from the photodiode was recorded by an Axopatch 200A amplifier and a Digidata-1550 digitizer controlled by pClamp10 (Molecular Devices, San Jose, CA, USA). H<sub>v1</sub> channels were activated by 1-s-long depolarizations to +100 mV (if other membrane potential is not indicated) from a holding potential of –60 mV to evoke the VCF signals.

For flavonoid mixture and Oxophench measurements, molecules were dissolved in DMSO at 100 mM (stock solution) and then diluted in extracellular solution to the appropriate concentration (10, 1, 0.1 and 0.01 μM).

Electrophysiological data analysis was performed using CLAMPFIT (v10; Molecular Devices), SIGMAPLOT (v10; Sigma-Stat Software, San Jose, CA, USA), and Excel (Microsoft, Redmond, WA, USA). Current and VCF signals were recorded at 2 kHz and low-pass filtered at 1 kHz. Fluorescence traces represent single recordings (without averaging) and were filtered with a Boxcar filter (smoothing points: 3). The magnitude of the VCF signals was expressed as Δ*F*/*F*<sub>h</sub> in percentage, where *F*<sub>h</sub> is the baseline fluorescence at the holding voltage of –60 mV, and Δ*F* is the change in fluorescence upon depolarization. Δ*F* can be quantified in different ways: Δ*F*<sub>peak</sub> is negative peak fluorescence change during the voltage step, Δ*F*<sub>ss</sub> (steady state) is the change in fluorescence at the end of the voltage step, Δ*F*<sub>tail</sub> is the maximum change in fluorescence during repolarization after the voltage step and Δ*F*<sub>hook</sub> = Δ*F*<sub>tail</sub> – Δ*F*<sub>ss</sub>; the relative fluorescence change: Δ*F*/*F*<sub>h</sub>, simplified to Δ*F*/*F*.

To correct for photobleaching, the baseline fluorescence trace, which has no change in voltage, was fitted with an exponential function. The parameters (amplitude and tau) of this fitting were used for photobleaching correction. *F*–*V* plots show the Δ*F*/*F*<sub>h</sub> values, normalized to the maximum value as a function of test potential. *G*–*V* curves were constructed by using the leak-corrected tail- or peak current measured during repolarization or depolarization, normalized to the minimum or maximum value, respectively, plotted as a function of test potential.

The inhibitory effect at a given concentration was calculated as the Remaining Current Fraction (RCF = *I*/*I*<sub>0</sub>), where *I*<sub>0</sub> is the peak current in the absence of Oxophench, and *I* is the peak current at equilibrium block at a given concentration of Oxophench. The data points (average of 5 individual records) in the dose–response curve was fitted with a three-parameter inhibitor vs. response model using

$$\text{RCF} = Y_{\min} + (1 - Y_{\min}) \frac{K_d^{n_H}}{K_d^{n_H} + [\text{Oxophench}]^{n_H}},$$

where Oxophench is the molar concentration of Oxophench, *K*<sub>d</sub> is the dissociation constant, and *n*<sub>H</sub> is the Hill coefficient. All data are presented as means ± SEM.



## Spectrofluorimetry

This method has been described in our earlier paper [6]. TAMRA-MTS was excited at 535 nm and the emission spectrum was measured in the 550–650 nm range, in the absence or presence of Oxophench, using a Spex Fluoromax (Jobin Yvon) spectrofluorimeter (<https://www.horiba.com/int/>). The recording solution was the same as the extracellular solution for VCF recordings, and the Oxophench was dissolved in this solution. TAMRA-MTS concentration was 20 nM. Measurements were performed at room temperature with continuous stirring right after mixing Oxophench with TAMRA-MTS (within 1 min). For control recordings, we measured the emission spectrum of the extracellular solution without TAMRA-MTS but with Oxophench at different concentrations. These control recordings were subtracted from the appropriate measurement data and plotted in the figures.

## Oxophench fluorescent labeling

Fluorescent staining was performed on wild-type HEK293 cells (RRID: CVCL\_0045; acquired from the American Type Culture Collection (Manassas, VA, USA); mycoplasma-free, regularly tested for it), cultured on glass-bottom dishes (Ibidi, Gräfelting, Germany) at 37 °C with 5% CO<sub>2</sub> in DMEM medium purchased from Sigma-Aldrich. Prior to labeling, cells were washed twice with PBS and then labeled with 10 μM Oxophench. Fluorescence imaging was performed at 37 °C using an imaging setup composed of a Zeiss AxioVert 100 inverted fluorescence microscope (Zeiss, Oberkochen, Germany) and a polychromator (Visitron Systems, Puchheim, Germany). As derived from the excitation and emission spectra of Oxophench (Fig. 2), samples were excited with 365 nm light for 100 ms. The filter set contained a dichroic mirror (ZT488rdc) and an emission filter ET525/50 m. For time-lapse measurements, images were taken every 5 s.

Fluorescent staining was performed on wild-type HEK293 cells, cultured on eight-well chambered coverslip (Ibidi) at 37 °C with 5% CO<sub>2</sub> in DMEM medium purchased from Sigma-Aldrich. Prior to labeling, cells were washed twice with PBS and then labeled with 10 μM Oxophench. Fluorescence imaging was performed at 37 °C using an LSM880 confocal laser-scanning microscope (Carl Zeiss AG, Jena, Germany). As derived from the excitation and emission spectra of Oxophench (Fig. 2), samples were excited at 405 nm and the emission was detected between 500 and 600 nm.

## Measurement of membrane fluidity

The effect of Oxophench on membrane fluidity was determined by quantifying fluorescence anisotropy of 4'-(trimethylammonio)-diphenylhexatriene (TMA-DPH, Sigma-Aldrich) using spectrofluorimetry as described previously [27,28]. Briefly, control HEK293 cells and those treated with 10 μM Oxophench were subsequently labeled with

10 μM TMA-DPH for 10 min at room temperature. Fluorescence intensities were measured without washing using a Fluorolog-3 spectrofluorimeter (Horiba Jobin Yvon, Edison, NJ, USA) with the temperature of the cuvette holder adjusted to 37 °C by a circulating water bath. TMA-DPH was excited at 352 nm and its emission was measured at 430 nm. Fluorescence anisotropy ( $r$ ) was measured in the L-format according to the formula

$$r = \frac{I_{VV} - GI_{VH}}{I_{VV} + 2GI_{VH}},$$

where  $I_{VV}$  and  $I_{VH}$  are the vertical and horizontal components, respectively, of the fluorescence excited by vertically polarized light, and  $G$  is an instrument-specific correction factor characterizing the different sensitivity of the detection system for vertically and horizontally polarized light:

$$G = \frac{I_{HV}}{I_{HH}},$$

where  $I_{HV}$  and  $I_{HH}$  are the vertical and horizontal components, respectively, of the fluorescence excited by horizontally polarized light.

## Molecular modeling

Modeling was performed as it was described before [6]. Briefly, we performed homology modeling of the CiHv1 (Uniprot ID: Q1JV40) transmembrane domains and interconnecting loops using the crystal structure of the mouse H<sub>v</sub>1 (PDB ID: 3WKV) as a template on the Swiss Model interface. Afterwards, we modified the E241 to Cys and appended the TAMRA-MTS to this Cys in different conformations using PYMOL (Developer(s) Schrödinger, Inc., <https://pymol.org/2/>). The protein model geometry was validated with the UCLA SAVES Ramachandran plot (Fig. 7) [31]. We created a 200 × 200 Å palmitoyl oleoyl phosphatidylcholine (POPC) model lipid bilayer using the CELLMI-croscosmos 2 MembraneEditor 2.2. Next, we embedded CiHv1 into the POPC membrane in an orientation resembling the X-ray crystal structure of mouse H<sub>v</sub>1 [32]. Following an energy minimization step, we visualized the surroundings of TAMRA-conjugated CiHv1 using UCSF CHIMERA X [33] and measured the distance of TAMRA to the cell membrane [34]. For docking Oxophench to the membrane-bound protein, we used AUTODOCK [35] and defined a bounding box on the extracellular part of the membrane/channel complex. The Oxophench molecule localized at the position with the lowest Gibbs free energy of binding was retained for the final model for illustrative purposes.

## Mathematical modeling

This method has been described in our earlier paper [6]. Fluorescence intensity at a given time point was calculated

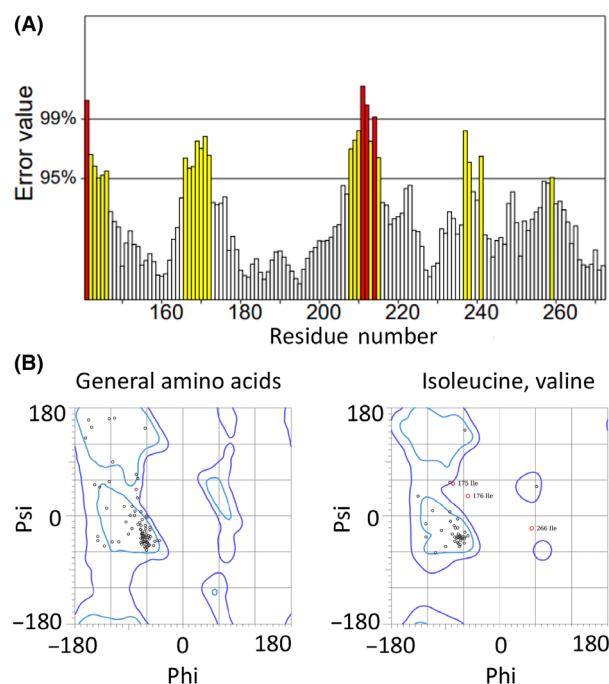


**Fig. 7.** Quality assessment of CiHv1-TAMRA model geometry. (A) Error values, based on the statistics of non-bonded atom-atom interactions in the reported structure, are plotted as a function of the amino acid position of a sliding 9-residue window. Regions of the structure that can be rejected at the 95% confidence level are yellow, i.e., 5% of a good protein structure is expected to have an error value above this level. Regions that can be rejected at the 99% level are shown in red. (B) Ramachandran plot of the model. Phi values on the x-axis and the Psi values on the y-axis to predict the possible conformation of the peptide. The angle spectrum in each axis is from  $-180^\circ$  to  $+180^\circ$ . The regions highlighted in dark and light blue show amino acids (black dots) in core and allowed conformations, respectively. The amino acids highlighted in red are outside the allowed conformation range.

as the following:  $F = \sum_{i=1}^3 P_i F_i$ , where  $P_i$  is the probability being in state “ $i$ ” and  $F_i$  is the fluorescence intensity in state “ $i$ ”. The transitions between states “ $i$ ” and “ $j$ ” were assumed to pass via an intermediate transition state “ $ij$ ” so the transition rate was then  $r_{ij}(t) = \exp(-(\Delta g_{ij} + \Delta q_{ij}V(t))/kT)/\tau$ , where  $\Delta g_{ij} = g_{ij} - g_i$  is the free energy difference at  $V = 0$  mV between states “ $i$ ” and “ $ij$ ”,  $\Delta q_{ij} = q_{ij} - q_i$  is the charge transferred across the membrane in moving from state “ $i$ ” to “ $ij$ ”,  $k$  is Boltzmann’s constant,  $T$  is the temperature, and  $\tau$  characterizes the timescale for a barrier-free reaction. The fluorescence intensities ( $F_i$ ), free energy ( $g_i, g_{ij}$ ), and charge ( $q_i, q_{ij}$ ), were then estimated via a non-linear, least squares fit to the experimental fluorescence measurements. The simplest model that adequately fitted allowed sequential transitions between  $N = 3$  states (i.e.  $1 \leftrightarrow 2 \leftrightarrow 3$ ).

## Statistics and reproducibility

Bar charts show mean values with individual data points. Reported errors are SEM, numbers of cells ( $n$ ) and the number of batches the cells originated from ( $N$ ) involved in the given analysis are shown in the text or in the figure.  $P$  values were calculated, after testing normal distribution of our samples, with a two-tailed Student’s  $t$ -test or ANOVA (one-way) analysis with a Holm-Sidak *post-hoc* test. Differences were considered significant (asterisk, \*) when  $P < 0.05$ . Measurements were taken from distinct samples (regarding Spectrofluorimetry) or from different oocytes (regarding VCF).

## Acknowledgements

We thank Gilman E. S. Toombes for performing the model calculations. We also thank Peter Larsson for the CiHv1 cDNA and members of our Electrophysiology group and Ion channel structure–function laboratory for helpful discussions. Molecular graphics and analyses performed with UCSF CHIMERAX, developed by the Resource for Biocomputing, Visualization, and Informatics at the University of California, San Francisco, with support from National Institutes of Health R01-GM129325 and the Office of Cyber Infrastructure and Computational Biology, National Institute of Allergy and Infectious Diseases. We would also like to thank Professor György Balla for his advice delivered at the 2022-ÚNKP conference. This work was supported by OTKA Bridging Fund 1G3DBKB0BFPP247 (FP); OTKA 132906 (ZV); 2019-2.1.11-TÉT-2019-00059 (ZV); by János Bolyai Research Scholarship of the Hungarian Academy of Sciences (BO/00355/21/8) (FP); by the ÚNKP-22-5-DE-420 New National Excellence Program of the Ministry for Innovation and Technology (FP). This study was also funded by the Slovenian Research Agency (Grant No. P1-0208) (NZ).

## Conflict of interest

The authors declare no conflict of interest.

## Author contributions

ZP, DP, MP, ZsM, FZ, TK, and FP performed the experiments. ZP and FP wrote the manuscript. ZP, FZ, TK, and FP analyzed the data and made figures. ZP, FZ, TK, and FP performed the statistical analysis. ZP and FP did the molecular biology work. ZP and FP designed the experiments. ZP, NZ, GP, ZV, and

FP revised the manuscript. All authors reviewed the manuscript.

## Peer review

The peer review history for this article is available at <https://www.webofscience.com/api/gateway/wos/peer-review/10.1111/febs.17105>.

## Data availability statement

The datasets generated and analyzed during the current study are available from the corresponding author upon reasonable request. The computer code and algorithm used to generate results that are reported in the paper are available from Gilman E. S. Toombes on reasonable request.

## References

- Gandhi CS & Olcese R (2008) The voltage-clamp fluorometry technique. *Methods Mol Biol* **491**, 213–231.
- Mannuzzo LM, Moronne MM & Isacoff EY (1996) Direct physical measure of conformational rearrangement underlying potassium channel gating. *Science* **271**, 213–216.
- Mony L, Berger TK & Isacoff EY (2015) A specialized molecular motion opens the Hv1 voltage-gated proton channel. *Nat Struct Mol Biol* **22**, 283–290.
- Pantazis A, Westerberg K, Althoff T, Abramson J & Olcese R (2018) Harnessing photoinduced electron transfer to optically determine protein sub-nanoscale atomic distances. *Nat Commun* **9**, 4738.
- Papp F, Lomash S, Szilagyi O, Babikow E, Smith J, Chang TH, Bahamonde MI, Toombes GES & Swartz KJ (2019) TMEM266 is a functional voltage sensor regulated by extracellular Zn(2). *Elife* **8**, e42372.
- Papp F, Toombes GES, Petho Z, Bagosi A, Feher A, Almasy J, Borrego J, Kuki A, Keki S, Panyi G et al. (2022) Multiple mechanisms contribute to fluorometry signals from the voltage-gated proton channel. *Commun Biol* **5**, 1131.
- Cha A & Bezanilla F (1997) Characterizing voltage-dependent conformational changes in the shaker K<sup>+</sup> channel with fluorescence. *Neuron* **19**, 1127–1140.
- Asamoah OK, Wuskell JP, Loew LM & Bezanilla F (2003) A fluorometric approach to local electric field measurements in a voltage-gated ion channel. *Neuron* **37**, 85–97.
- Klymchenko AS & Demchenko AP (2002) Electrochromic modulation of excited-state intramolecular proton transfer: the new principle in design of fluorescence sensors. *J Am Chem Soc* **124**, 12372–12379.
- Klymchenko AS, Stoeckel H, Takeda K & Mely Y (2006) Fluorescent probe based on intramolecular proton transfer for fast ratiometric measurement of cellular transmembrane potential. *J Phys Chem B* **110**, 13624–13632.
- Wen K, Fang X, Yang J, Yao Y, Nandakumar KS, Salem ML & Cheng K (2021) Recent research on flavonoids and their biomedical applications. *Curr Med Chem* **28**, 1042–1066.
- Pajtas D, Konya K, Kiss-Szikszai A, Dzubak P, Petho Z, Varga Z, Panyi G & Patonay T (2017) Optimization of the synthesis of flavone-amino acid and flavone-dipeptide hybrids via Buchwald-Hartwig reaction. *J Org Chem* **82**, 4578–4587.
- Wloch A, Strugala-Danak P, Pruchnik H, Krawczyk-Lebek A, Szczeka K, Janeczko T & Kostrzewa-Suslow E (2021) Interaction of 4'-methylflavonoids with biological membranes, liposomes, and human albumin. *Sci Rep* **11**, 16003.
- Selvaraj S, Krishnaswamy S, Devashya V, Sethuraman S & Krishnan UM (2015) Influence of membrane lipid composition on flavonoid-membrane interactions: implications on their biological activity. *Prog Lipid Res* **58**, 1–13.
- Zakany F, Kovacs T, Panyi G & Varga Z (2020) Direct and indirect cholesterol effects on membrane proteins with special focus on potassium channels. *Biochim Biophys Acta Mol Cell Biol Lipids* **1865**, 158706.
- Orts DJB & Arcisio-Miranda M (2022) Cell glycosaminoglycans content modulates human voltage-gated proton channel (H(V) 1) gating. *FEBS J* **289**, 2593–2612.
- Richter-Laskowska M, Trybek P, Delfino DV & Wawrzekiewicz-Jalowicka A (2023) Flavonoids as modulators of potassium channels. *Int J Mol Sci* **24**, 1311.
- Chae MR, Kang SJ, Lee KP, Choi BR, Kim HK, Park JK, Kim CY & Lee SW (2017) Onion (*Allium cepa* L.) peel extract (OPE) regulates human sperm motility via protein kinase C-mediated activation of the human voltage-gated proton channel. *Andrology* **5**, 979–989.
- Schoefer L, Braune A & Blaut M (2001) A fluorescence quenching test for the detection of flavonoid transformation. *FEMS Microbiol Lett* **204**, 277–280.
- Liu Z, Balasubramanian V, Bhat C, Vahermo M, Makila E, Kemell M, Fontana F, Janoniene A, Petrikaite V, Salonen J et al. (2017) Quercetin-based modified porous silicon nanoparticles for enhanced inhibition of doxorubicin-resistant cancer cells. *Adv Healthc Mater* **6**, doi: 10.1002/adhm.201601009
- Papadopoulou A, Green RJ & Frazier RA (2005) Interaction of flavonoids with bovine serum albumin: a fluorescence quenching study. *J Agric Food Chem* **53**, 158–163.

- 22 Sett R, Paul BK & Guchhait N (2021) Deciphering the fluorescence quenching mechanism of a flavonoid drug following interaction with human hemoglobin. *J Phys Org Chem* **35**, e4307.
- 23 Ramsey IS, Moran MM, Chong JA & Clapham DE (2006) A voltage-gated proton-selective channel lacking the pore domain. *Nature* **440**, 1213–1216.
- 24 Sasaki M, Takagi M & Okamura Y (2006) A voltage sensor-domain protein is a voltage-gated proton channel. *Science* **312**, 589–592.
- 25 Qiu F, Rebolledo S, Gonzalez C & Larsson HP (2013) Subunit interactions during cooperative opening of voltage-gated proton channels. *Neuron* **77**, 288–298.
- 26 Wu K, Zhao Z, Wang R & Wei GW (2018) TopP-S: persistent homology-based multi-task deep neural networks for simultaneous predictions of partition coefficient and aqueous solubility. *J Comput Chem* **39**, 1444–1454.
- 27 Zakany F, Szabo M, Batta G, Karpati L, Mandity IM, Fulop P, Varga Z, Panyi G, Nagy P & Kovacs T (2021) An omega-3, but not an omega-6 polyunsaturated fatty acid decreases membrane dipole potential and stimulates Endo-lysosomal escape of penetratin. *Front Cell Dev Biol* **9**, 647300.
- 28 Kovacs T, Sohajda T, Szente L, Nagy P, Panyi G, Varga Z & Zakany F (2021) Cyclodextrins exert a ligand-like current inhibitory effect on the K(V)1.3 ion channel independent of membrane cholesterol extraction. *Front Mol Biosci* **8**, 735357.
- 29 Chen H, Ahsan SS, Santiago-Berrios MB, Abruna HD & Webb WW (2010) Mechanisms of quenching of Alexa fluorophores by natural amino acids. *J Am Chem Soc* **132**, 7244–7245.
- 30 Zakany F, Pap P, Papp F, Kovacs T, Nagy P, Peter M, Szente L, Panyi G & Varga Z (2019) Determining the target of membrane sterols on voltage-gated potassium channels. *Biochim Biophys Acta Mol Cell Biol Lipids* **1864**, 312–325.
- 31 Colovos C & Yeates TO (1993) Verification of protein structures: patterns of nonbonded atomic interactions. *Protein Sci* **2**, 1511–1519.
- 32 Takeshita K, Sakata S, Yamashita E, Fujiwara Y, Kawanabe A, Kurokawa T, Okochi Y, Matsuda M, Narita H, Okamura Y *et al.* (2014) X-ray crystal structure of voltage-gated proton channel. *Nat Struct Mol Biol* **21**, 352–357.
- 33 Pettersen EF, Goddard TD, Huang CC, Meng EC, Couch GS, Croll TI, Morris JH & Ferrin TE (2021) UCSF ChimeraX: structure visualization for researchers, educators, and developers. *Protein Sci* **30**, 70–82.
- 34 Sommer B, Dingersen T, Gamroth C, Schneider SE, Rubert S, Kruger J & Dietz KJ (2011) CELLmicrocosmos 2.2 MembraneEditor: a modular interactive shape-based software approach to solve heterogeneous membrane packing problems. *J Chem Inf Model* **51**, 1165–1182.
- 35 Morris GM, Huey R, Lindstrom W, Sanner MF, Belew RK, Goodsell DS & Olson AJ (2009) AutoDock4 and AutoDockTools4: automated docking with selective receptor flexibility. *J Comput Chem* **30**, 2785–2791.